

Monthly Representations of Mid-Tropospheric Carbon Dioxide from the Atmospheric Infrared Sounder

Thomas S. Pagano^{a*}, Edward T. Olsen^a, Moustafa T. Chahine^a, Alexander Ruzmaikin^a,
Hai Nguyen^a, Xun Jiang^b

^aCalifornia Institute of Technology, Jet Propulsion Laboratory,
4800 Oak Grove Drive, Pasadena, CA, USA 91109

^bDepartment of Earth and Atmospheric Sciences, University of Houston, Houston, Texas, USA

ABSTRACT

The Atmospheric Infrared Sounder (AIRS) on NASA's Earth Observing System Aqua spacecraft was launched in May of 2002 and acquires hyperspectral infrared spectra used to generate a wide range of atmospheric products including temperature, water vapor, and trace gas species including carbon dioxide. Here we present monthly representations of global concentrations of mid-tropospheric carbon dioxide produced from 8 years of data obtained by AIRS between the years of 2003 and 2010. We define them as "representations" rather than "climatologies" to reflect that the files are produced over a relatively short time period and represent summaries of the Level 3 data. Finally, they have not yet been independently validated. The representations have a horizontal resolution of $2.0^\circ \times 2.5^\circ$ (Latitude \times Longitude) and faithfully reproduce the original 8 years of monthly L3 CO₂ concentrations with a standard deviation of 1.48 ppm and less than 2% outliers. The representations are intended for use in studies of the global general circulation of CO₂ and identification of anomalies in CO₂ typically associated with atmospheric transport. The seasonal variability and trend found in the AIRS CO₂ data are discussed.

Keywords: Atmospheric Infrared Sounder, Aqua Spacecraft, Carbon Dioxide

1. INTRODUCTION

The Atmospheric Infrared Sounder (AIRS) is a hyperspectral infrared instrument on the EOS Aqua Spacecraft, launched on May 4, 2002 (Aumann et al., 2003). AIRS has 2378 infrared channels ranging from 3.7 μm to 15.4 μm , and a 13.5 km footprint at nadir and scans $\pm 49.5^\circ$ from an orbit altitude of 705.3 km, covering 95% of the globe every day. AIRS, in conjunction with the Advanced Microwave Sounding Unit (AMSU), produces temperature profiles with 1K/km accuracy on a global scale, as well as water vapor profiles and trace gas amounts for CO₂, CO, SO₂, O₃, and CH₄. AIRS data are used for weather forecasting, climate process studies, and validating climate models.

Several international groups have successfully retrieved concentrations of mid-tropospheric CO₂ from AIRS (Pagano et al., 2011). The CO₂ data used in this analysis are produced by the NASA AIRS Project and are unique in a sense of global spatial coverage, i.e. not being limited to only clear sky regions. The data are produced using the method of Vanishing Partial Derivatives (VPD) (Chahine et al., 2005). The VPD method solves for the least squares CO₂ estimates by iteratively minimizing the difference between the observed cloud-cleared radiances and calculated radiances for AIRS using the AIRS Radiative Transfer Algorithm (RTA). The VPD is based on coordinate descent methodology, that is, it applies the minimization independently and sequentially to all geophysical parameters that impact the radiance of a given channel used to retrieve CO₂, e.g., atmospheric temperature, water vapor, ozone, and carbon dioxide. The process is iterated until the radiance residuals for all parameters are minimized or the change in CO₂ falls below 0.25 ppm. Extensive quality control is applied during the retrieval including: quality of the AIRS geophysical products, monotonically decreasing radiance residuals from one iteration to the next, and spatial homogeneity of a 2×2 set of retrievals (clusters) required to be within 2 ppm in an RMS sense. The resulting "Level 2" product achieves a yield of over 15,000 mid-tropospheric CO₂ retrievals per 24-hour period, each with a horizontal footprint of 90×90 km centered over the area where acquired.

AIRS Level 2 CO₂ retrievals were compared to aircraft measurements made in the mid-troposphere by Matsueda, taken over the Pacific Ocean at ≥ 10 km altitude between Australia and Japan from Sept. 2002 to March 2004 (Chahine et al., 2005). Comparisons of the individual AIRS CO₂ daily concentrations to the concentrations measured by Matsueda give

*tpagano@jpl.nasa.gov, (818) 393-3917, <http://airs.jpl.nasa.gov>

a Root Mean Square (RMS) deviation of less than 3.0 ppm with a bias of approximately 1.0 ppm. The distribution of differences is Gaussian allowing accuracy improvement due to averaging in the monthly data products. For 7 clusters used in a month, the RMS error is 1.2 ppm with a bias of 0.4 ppm. The AIRS Level 3 (L3) Monthly Gridded CO₂ data files were not compared directly with Matsueda's data but are generated as a simple averaging of the valid Level 2 data points in the grid location and timeframe. Considerably more samples are included in each bin of the L3 data product, depending on location, so we can expect smaller biases and improved accuracy due to averaging as demonstrated prior.

Comparisons to other data sets including the Intercontinental Chemical Transport Experiment –North America (INTEX-NA) measurements during July 2004 and upward looking Fourier Transform Infrared Spectrometers (FTIR) measurements show comparable accuracies as demonstrated with the Matsueda data (Chahine et al., 2008). Also in this study, AIRS mid-tropospheric CO₂ data have shown higher than expected variability that can be associated with geophysical phenomenon. Temporal variability can be seen associated with the seasonal drawdown of CO₂ by the global biomass. Horizontal variability at the continental scale associated with the known sources of CO₂ and the circulation of the jet stream can be clearly seen. In certain cases (e.g., El Niño) observations of increased CO₂ levels in the mid-troposphere can be associated with upwelling air. Higher levels of CO₂ in the mid-troposphere commensurate with reduced mid-tropospheric ozone levels are seen in AIRS data at high latitudes that can be associated with sudden stratospheric warming events.

To our knowledge, there is no representation or climatology of global CO₂ concentrations in the mid-troposphere obtained from direct observation. Many studies have been done to date that show the potential value of AIRS mid-tropospheric CO₂ representations to facilitate model comparison and identification of anomalies associated with weather and climate patterns. In one study, anomalies in detrended AIRS mid-tropospheric CO₂ concentrations were used to observe climate related processes in the polar region and due to the El Niño–Southern Oscillation (ENSO) (Jiang et al., 2010). Anomalies in AIRS mid-tropospheric CO₂ L3 data were used to identify large-scale vertical atmospheric motion associated with the Madden Julian Oscillation (MJO) (Li et al., 2010). This latter study clearly showed the correlation of mid-tropospheric CO₂ concentrations and upwelling air, suggesting a vertical difference of CO₂ from the surface to the mid-troposphere of about 0.67 ± 0.26 ppm. One of the first comparisons of AIRS derived mid-tropospheric CO₂ (albeit from a different retrieval) was with the TM3 and LMDZ models (Tiwari et al., 2006). A second, more recent study found good agreement of GEOS-5 mid-tropospheric CO₂ concentrations compared to AIRS L3 CO₂ in northern latitudes, with smaller seasonal cycle and lower concentrations than AIRS in the southern hemisphere (Feng et al., 2011). In general it is believed that a well-characterized set of monthly mid-tropospheric representations will facilitate research involving mid-tropospheric CO₂ and identify statistical significance of the observed variability and trends in the data.

2. METHOD

The objective is to develop a set of 12 monthly representations of the entire 8 years of AIRS CO₂ data. We require the reconstruction to be performed for each location i,j on a $2.0^\circ \times 2.5^\circ$ grid, and time, $k = 1, 2, \dots, N$, relative to $t_1 =$ January 2003 and follow the equation

$$C'_{ijk} = Z_{ijm} + \mu_{ij}(t_k - t_1),$$

where C'_{ijk} is the reconstructed CO₂ concentrations for the i^{th} latitude, j^{th} longitude, and k^{th} month, Z_{ijm} is the representation of the CO₂ concentrations for m^{th} month, where $m = k - (\text{floor}(k-1)/12)*12$, i.e., runs from 1 to 12, μ_{ij} is the rate of growth of CO₂ concentrations, or trend, and t_k is the date in fractional years of k^{th} month in the reconstructed series. A linear regression is performed over 8 years of measured AIRS L3 monthly gridded CO₂ data files for each month, m , to derive the trend, μ_{ijm} , and intercepts, A_{ijm} , for each location

$$C_{ijk} = A_{ijm} + \mu_{ijm}(t_k - t_1).$$

where C_{ijk} is the average monthly AIRS L3 CO₂ concentration at location i,j and month m . The monthly data files also include the standard deviation, σ_{ijk} , and number of samples in the corresponding bin, N_{ijk} . The trend is averaged over all months to remove the seasonal variability

$$\mu_{ij} = \sum_{m=1}^{12} \mu_{ijm}.$$

The intercepts, A_{ijm} , can be used as the monthly mean representations, however, a better method discussed in the next section was used that results in lower global variance.

3. MONTHLY MEAN CO₂ REPRESENTATIONS

The method we use to compute the monthly mean CO₂ representations starts with detrending the L3 Monthly Gridded CO₂ products using the trend derived above

$$D_{ijk} = C_{ijk} - \mu_{ij}(t_k - t_1).$$

The monthly mean CO₂ representations are simply the average of the detrended data sets over the $N = 8$ years of data

$$Z_{ijm} = \frac{1}{N} \sum_{n=1}^N D_{ijl_n},$$

where the annual data index for a given month, m , is $l_n = m + (n-1)*12$.

Figure 1 shows a Hovmöller diagram of detrended AIRS L3 monthly gridded CO₂ concentrations. The detrended data highlight features discussed earlier (Pagano et al., 2011) including the regular seasonal variability in the data, the time lag of CO₂ buildup in the Southern Hemisphere, and a band of reduced CO₂ in the Southern Hemisphere tropics. Figure 2 shows the representations derived from the AIRS data. We see a distinct seasonal cycle in the AIRS data that is repeated every year. The statistical significance of this cycle will be examined in the next section. Figure 3 shows the zonal average CO₂ concentrations from the representations. The monthly variability is highest in the northern latitudes with a clear and consistent dip in the concentrations in the Southern Hemisphere tropics.

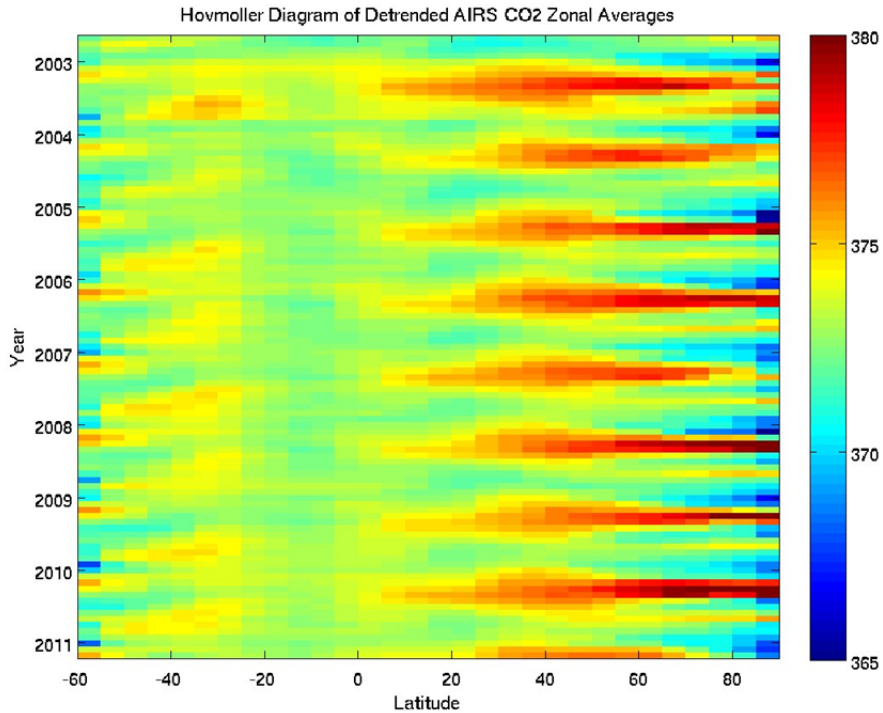


Figure 1. Hovmöller diagram of detrended AIRS mid-Tropospheric CO₂ shows the seasonal cycle. One can see the latitudinal gradient of CO₂, the larger concentration in the Northern Hemisphere compared with the concentration in the Southern Hemisphere, and a distinct band of lower CO₂ concentrations in the Southern Hemisphere tropics.

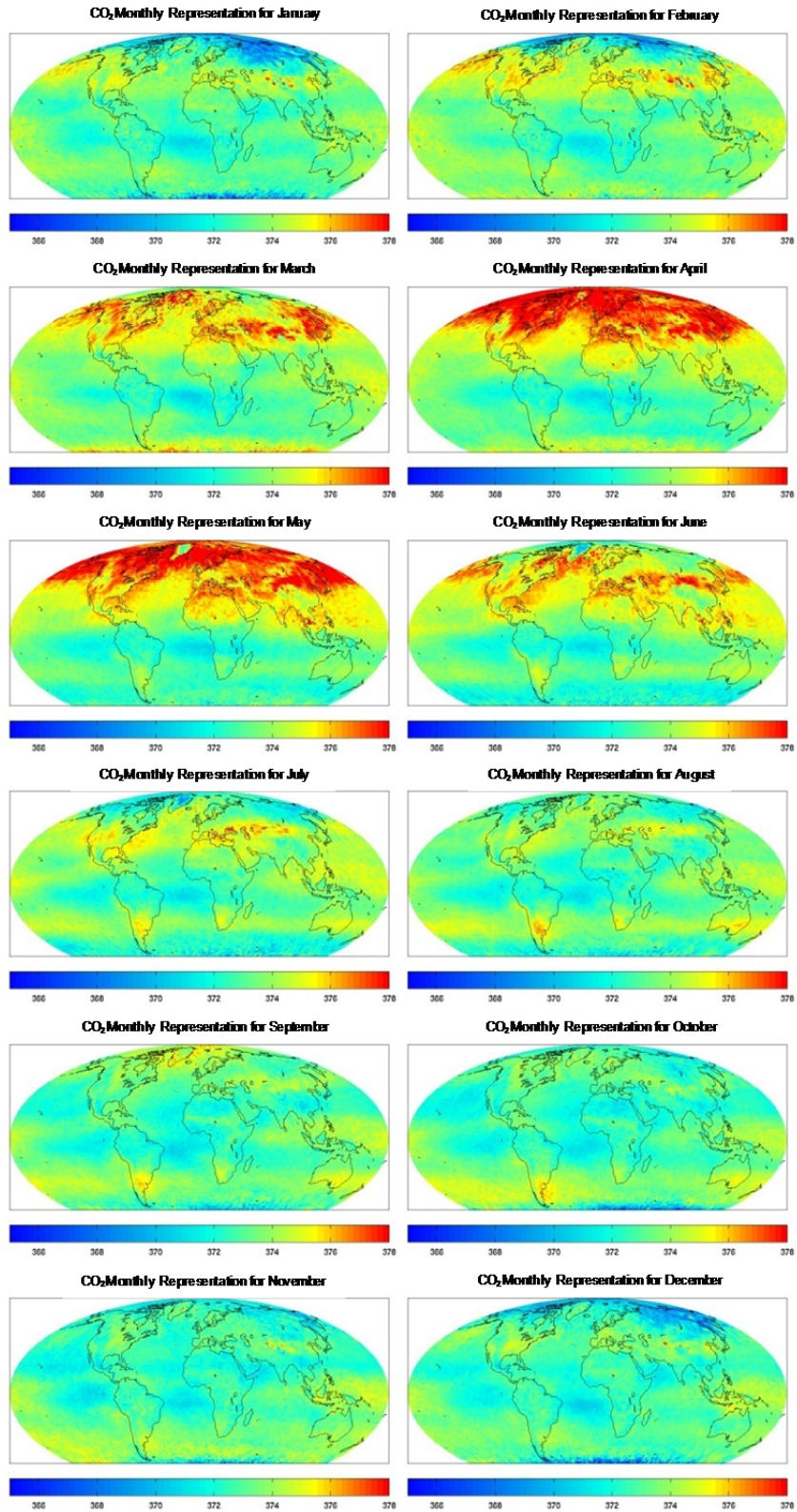


Figure 2. Monthly representations of mid-tropospheric CO₂ concentrations from the Atmospheric Infrared Sounder. The range of horizontal variability is on the order of 10 ppm and is highly repeatable every year.

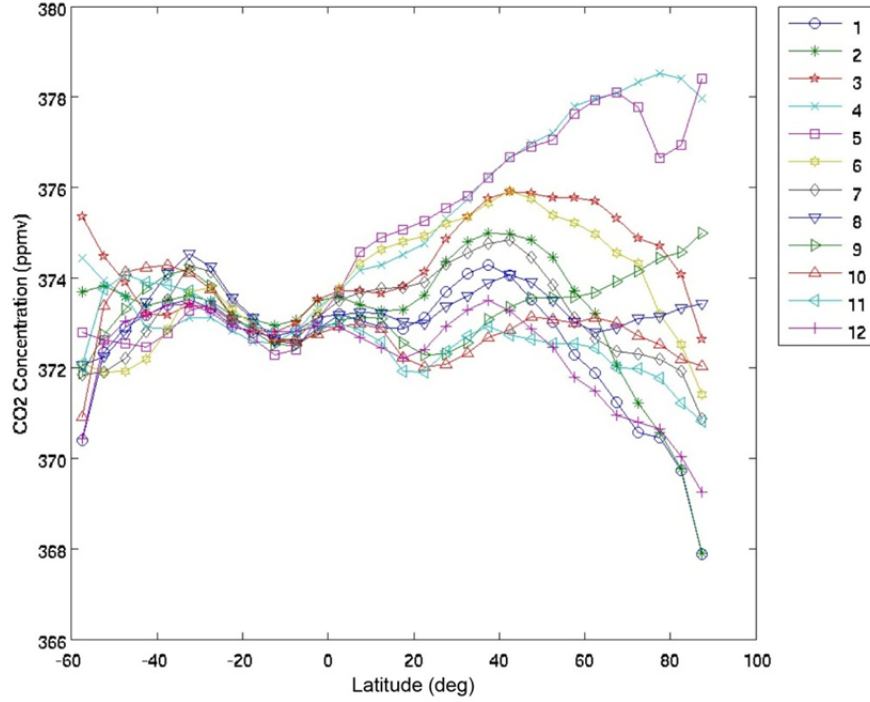


Figure 3. Zonal dependence of the AIRS mid-tropospheric CO₂ concentrations for each month. The data show a persistent drop in CO₂ concentrations in the Southern Hemisphere tropics with high seasonal variability in the northern latitudes.

The standard deviation in the CO₂ representations at any location for a given month combines the standard deviation in the original L3 monthly gridded CO₂ data sets using the number of counts from the L3 and the detrended CO₂ concentrations

$$\sigma_{Zijm} = \sqrt{\frac{\sum_{n=1}^N N_{ijl_n} [D_{ijl_n}^2 + \sigma_{ijl_n}^2]}{\sum_{n=1}^N N_{ijl_n}}} - D_{ijm}^2,$$

where

$$D_{ijm} = \frac{\sum_{n=1}^N N_{ijl_n} D_{ijl_n}}{\sum_{n=1}^N N_{ijl_n}}.$$

Figure 4 (top) shows the horizontal variability of the standard deviations for a typical representation, July. We see greater values in the polar region most likely due to the greater noise in the L3 data but also due to higher interannual variability in these regions.

The total number of observations represented in the CO₂ averages for a given month and location is the sum of all counts represented in the L3 files over all years

$$N_{ijm} = \sum_{n=1}^N N_{ijl_n}.$$

Figure 4 (bottom) shows the number of observations used to make the July representation. The counts of valid observations in the L3 files vary widely from 0 to 150, mostly due to cloud effects in the Level 2 retrieval. We see similar variability in the representation for July with values ranging from 0 to 1000. Locations with no valid L3 retrievals over the entire ensemble are set to -9999. The pattern of valid observations is independent CO₂ retrievals (i.e., does not introduce biases), however the fewer observations may affect the statistical significance in some areas.

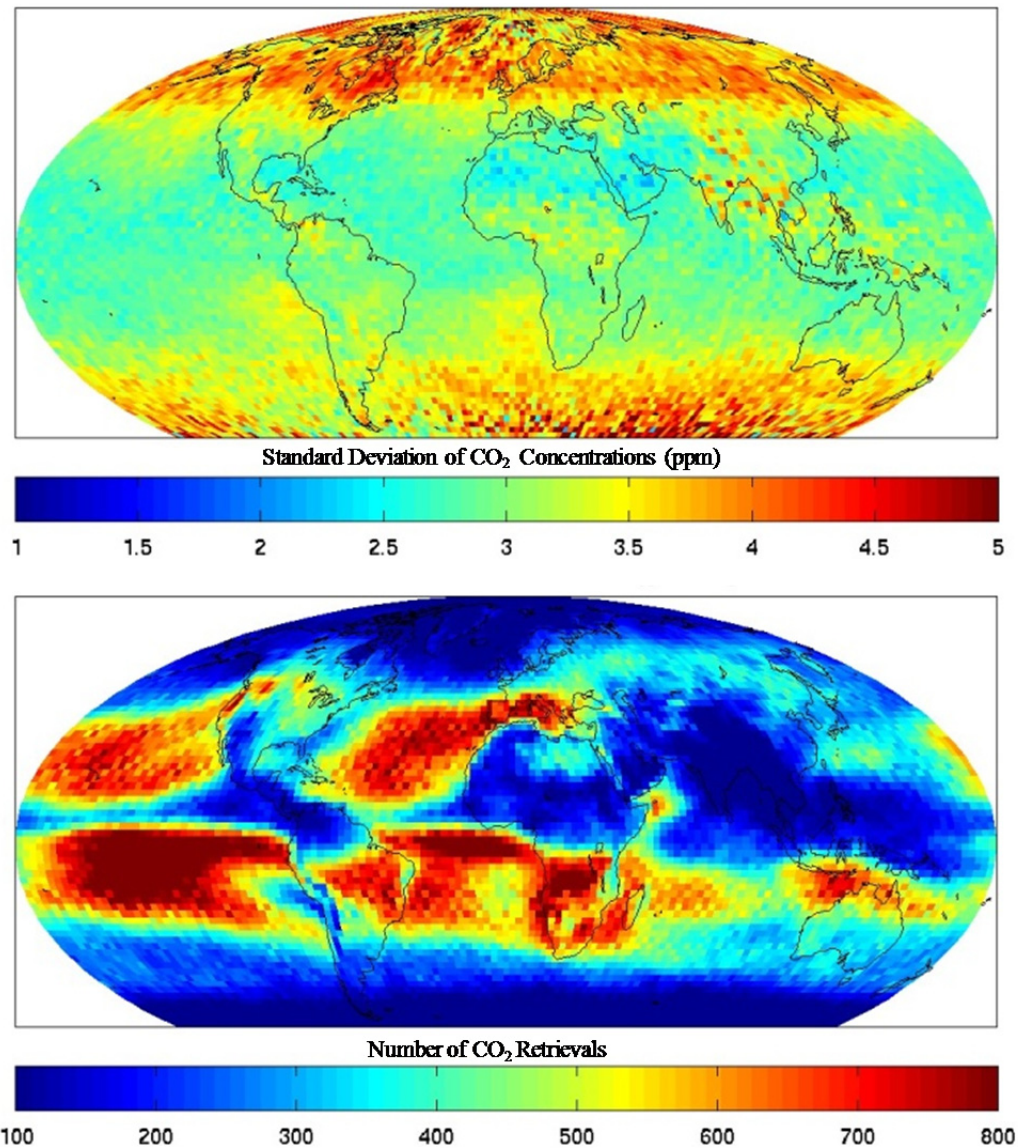


Figure 4. Top: Standard deviation of CO₂ concentrations for the July monthly representation. Bottom: Number of L3 retrievals used in the construction of the July monthly representation.

Figure 5 compares the original L3 data set (top) to the reconstructed zonal average CO₂ concentrations (bottom) obtained from the representations which, are also averaged over the specified zones. Zone width is 5°. The seasonal variability is more readily apparent in the reconstructions than in the original data. We see amplitude and phase dependence of the CO₂ most likely due to surface CO₂ from the biosphere. There is more CO₂ in the winter season and less CO₂ in the summer season. Transport will also modify the amplitude and phase of the CO₂ seasonal cycle.

The CO₂ monthly representations derived in this method reconstruct the original L3 monthly gridded CO₂ concentrations with a global standard deviation of 1.48 ppm over a population of 1,092,793 comparisons. 20,846 L3 CO₂ values are found exceeding 3-sigma for an outlier percentage of 1.9%. Reconstruction errors are shown in Figure 6 as a function of time from beginning of the mission. In this plot we show every month, and average over all longitudes. Note: using the intercepts for the representations results in a standard deviation between the reconstruction and original L3 data set of 1.74 ppm with 1.8% outliers.

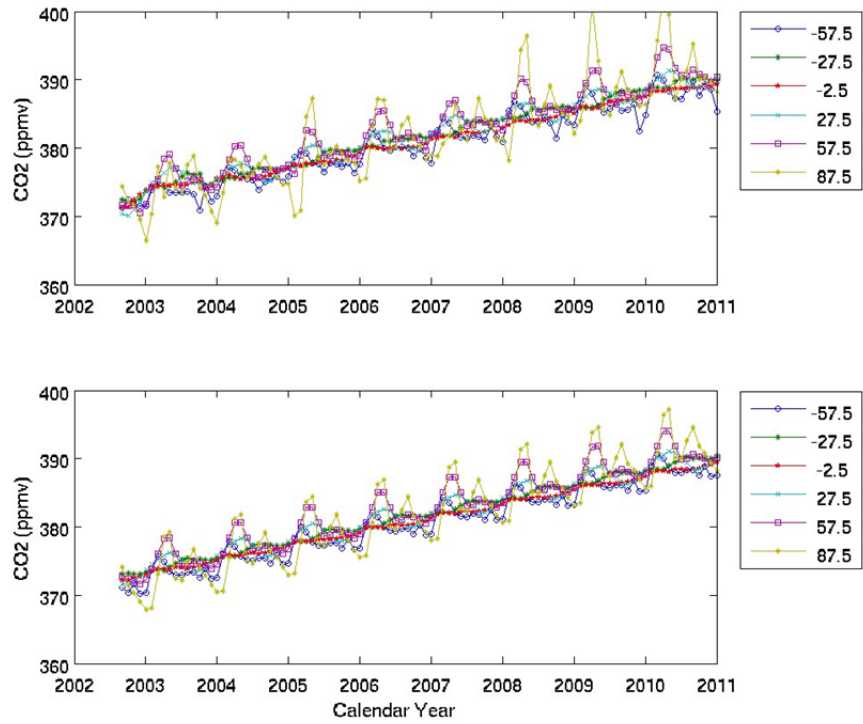


Figure 5. Time dependence of zonally averaged CO₂ concentrations for original AIRS L3 data sets (top panel) and reconstructed representations (bottom panel). Width of zone is 5°. Zones sampled are identified in the legend. The reconstructions show variability in the amplitude and phase of the seasonal signal of CO₂.

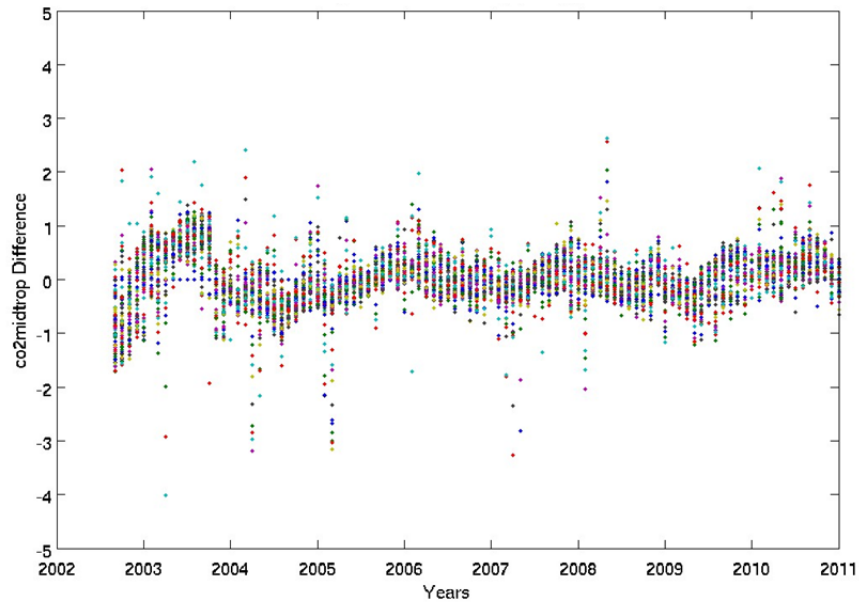


Figure 6. Reconstruction residuals of AIRS CO₂ representations (difference between L3 monthly gridded CO₂ and reconstruction based on representations). Data are shown for each month in the available time series, and for each of the 91 latitudes, averaged over all longitudes.

4. STATISTICAL SIGNIFICANCE OF SEASONAL VARIABILITY

The horizontal variability in the AIRS data for a given month is on the order of the seasonal variability or more. Significant increases in CO₂ concentrations occur in the Arctic region during the Northern Hemisphere spring that break up in the summer. The question is what is the statistical significance of this variability in the presence of measurement noise and interannual variability? We calculate the t -score for any given month with null hypothesis being that the monthly representations equal the annual means

$$T_{ijm} = \frac{Z_{ijm} - \bar{Z}_{ij}}{\frac{\sigma_{Z_{ijm}}}{\sqrt{N_{ijm}}}}$$

Using the t -score, and the degrees of freedom, $v_{ijm} = N_{ijm} - 1$, we can calculate the probability of obtaining a t -score as least as extreme as observed, given that the null hypothesis is true. This probability is related to the critical value, α_{ijm} representing the statistical significance. We use the MATLAB t -score cumulative distribution function to obtain the critical value for a 2-sided Student's-t test,

$$\alpha_{ijm} = 2 - 2 \text{tcdf}(|T_{ijm}|, v_{ijm}).$$

A plot of the zonal average critical value for each month is given in Figure 7. The majority of values are within an 80% probability (20% critical value). January and February have slightly higher critical values since the representations for these months are very close to the annual average leading to less significant differences from the annual mean and lower t -scores. While these results validate the statistical significance the horizontal seasonal variability in the AIRS CO₂ monthly representations, the accuracy of these representations is subject to a more thorough analysis of the spatial covariance and in-situ validation as done with the Level 2 data (e.g., Chahine et al., 2005; Chahine et al., 2008; Bai et al., 2010). Temporal covariance errors are mitigated by calculating the trend for each of the 12 months individually over the 8-year period then averaging the trends.

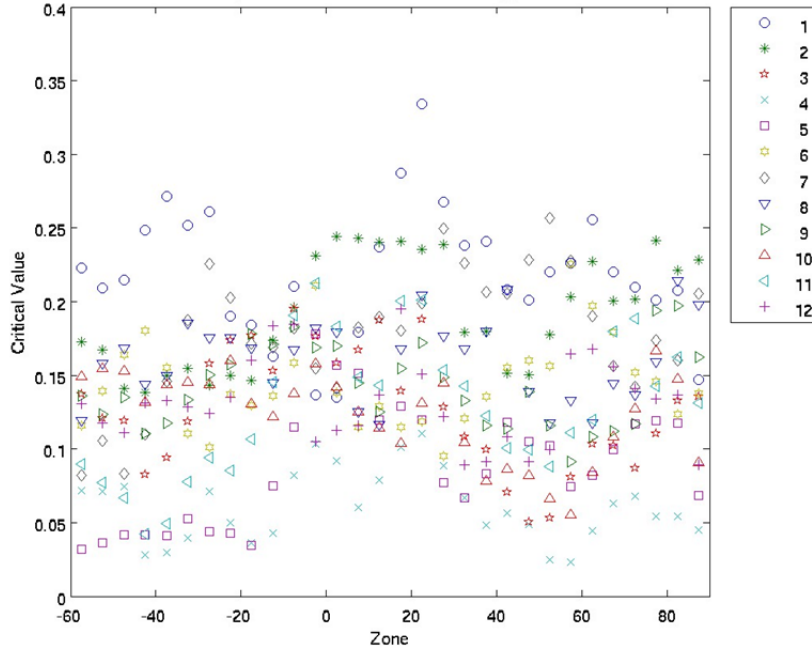


Figure 7. Zonal average of the critical value determined from the cumulative t -score representing the significance of the horizontal variability in the AIRS mid-tropospheric CO₂ representations relative to the annual mean. January and February representations are close to the annual mean, resulting in a higher critical value.

5. TRENDS AND UNCERTAINTY

The latitudinal variability of the trends in the AIRS data as derived above, μ_{ij} , if statistically significant, should be representative of the influence of surface sources and sinks on the mid-troposphere. Seasonal variability is removed in our calculation by determining the trend on each month then averaging the trends over all months. Another assumption is that the interannual trends (for a given month) are small compared to the trends due to sources and sinks.

The uncertainty in the trend, is typically given by the standard least-squared error for the slope,

$$\sigma_{\mu_{ijm}} = \sqrt{\frac{1}{N-2} \frac{\sum_{n=1}^N (C_{ijl_n} - C'_{ijl_n})^2}{\sum_{n=1}^N (t_{l_n} - \bar{t})^2}}.$$

This method produces a standard error in the slope, $\sigma_{\mu_{ijm}}$, of 0.15 ppm/year in the tropics to 0.25 ppm/year in the extra tropics (to 40° latitude). While this method will suffice, a more accurate method for determining uncertainty in the trend, includes the serial correlation in the data (Weatherhead et al., 1998),

$$\sigma_{\mu_{ijm}} = \frac{\sigma_{D_{ijm}}}{Y_{ij}^{3/2}} \sqrt{\frac{1 + \phi_{ijm}}{1 - \phi_{ijm}}},$$

where $\sigma_{D_{ijm}}$ is the noise of the CO₂ observations calculated for each month over the $Y_{ij}=8$ years of data after detrending,

$$\sigma_{D_{ijm}} = \frac{1}{N-1} \sqrt{\sum_{n=1}^N [D_{ijl_n}^2 - \bar{D}_{ijm}^2]},$$

and the autocorrelation function for lag = 1 is,

$$\phi_{ijm} = \frac{\sum_{n=1}^{N-1} (D_{ijl_n} - \bar{D}_{ijm})(D_{ijl_{n+1}} - \bar{D}_{ijm})}{\sum_{n=1}^N (D_{ijl_n} - \bar{D}_{ijm})}.$$

This method produces a standard error in the slope, $\sigma_{\mu_{ijm}}$, of approximately 0.1 ppm/year in the tropics to 0.2 ppm/year in the extra tropics and much worse in the polar region.

A map of the trends, μ_{ij} , and standard error combined over all months (as done for the standard deviation of the representation), $\sigma_{\mu_{ij}}$, is given in Figure 8. The total number of observations for any given location, M_{ij} that contribute to the slope is then $Y_{ij} \times 12 = 96$. The trends have a small amount of horizontal variability that is suggestive of surface sinks over large scale regions of high vegetation (e.g., Amazon, South Africa). However the variability is on the order of the standard error, indicating marginal statistical significance at this resolution for most of the globe. The trend is maintained as a per-location value in the representations to preserve as much accuracy in the reconstruction as possible.

To improve the significance, we can look at zonal averages. Figure 9 shows the zonal average trend over 5° latitude bins plotted with the standard deviation of the individual samples within each zone. The horizontal line is the global trend of 2.17 ppm/year obtained from the data. The bias error of the zonal trend in the tropics is approximately 0.002 ppm/year corresponding to a standard deviation of 0.3 ppm/year for individual samples in the zones divided by the square root of the approximately 40,000 samples in the zone. The bias error in northernmost arctic zone is approximately 0.01 ppm/year. The uncertainties plotted do not reflect the statistical improvement by averaging samples within the zone since we have not demonstrated the absence of horizontal correlated errors. Assuming all grid points are independent, and no biases in the L3 CO₂ trends, the zonal trends observed are statistically significant and show lower CO₂ rates of growth near the equatorial regions and higher rates of growth in the northern latitudes. This is expected as the major sources of anthropogenic CO₂ are in the northern hemisphere. Another possibility is that we are seeing trends caused by latitudinal transport, and while we attempt to mitigate this by calculating trends based on a given month then averaging the trends over all months, ongoing efforts by the authors including Empirical Orthogonal Function (EOF) analysis (Ruzmaikin, Aumann and Pagano, 2011 submitted to *J. Climate*) will characterize the spatial covariance of the representations to identify the significance of this possibility. In addition, further validation is needed to confirm the significance of trends, particularly in the polar region.

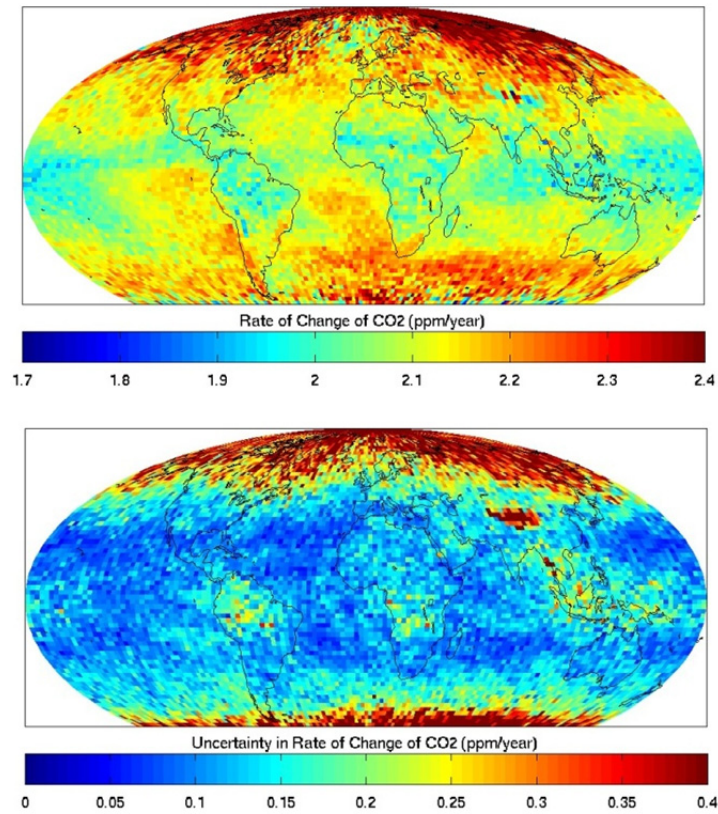


Figure 8. Top: Trends of AIRS CO₂ obtained by fitting the L3 monthly gridded data. Bottom: Standard errors in the trends are typically less than 0.15 ppm/year, except in the polar region.

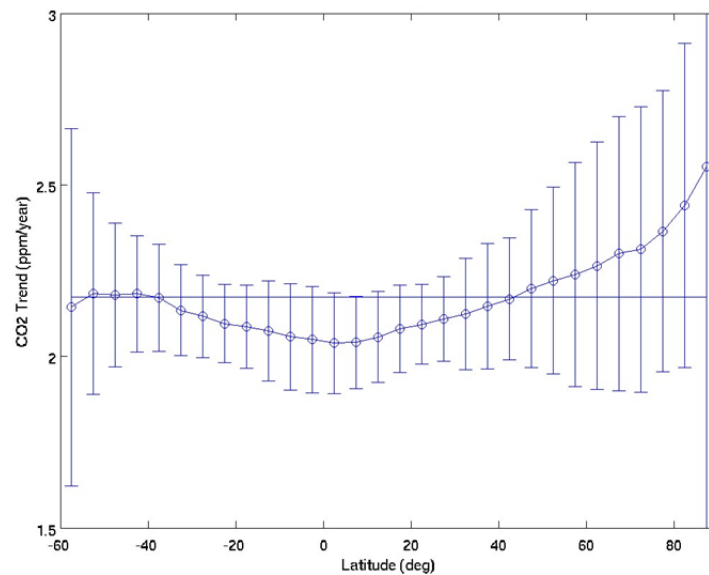


Figure 9. Zonal average trend shows lower values in the tropics and higher values in the northern latitudes. Error bars represent one-sigma variability of individual samples in zone. Significance of the trend at the zonal scale is high, however a more rigorous statistical significance test involving analysis of the spatial covariance is pending. The horizontal line is the global average of 2.17 ppm/year.

6. DATA FORMAT AND ACCESS

The representations are stored in a single text file containing the mean, standard deviation, and number of points of CO₂ for each of the twelve months. Provided after the CO₂ mean, standard deviation, and number of points are the trend matrix, intercept averaged over all months (not used in the reconstruction), uncertainty in the trend, and number of points used in determining each trend. The format of the file is given in Table 1. -9999 is given for all values (including Longitude and Latitude) for Latitudes less than -60°.

Table 1. Variables included in the representation file, their dimensions and typical values. Shaded areas are not included in the file.

Variable Name	0	0	Longitude (1 × 144)	Typical Value
Z_{ij1}	Month 1	Latitude (91 × 1)	CO ₂ Concentration (91 × 144)	372.5 ppm
Z_{ij2}	Month 2	Latitude (91 × 1)	CO ₂ Concentration (91 × 144)	373.2 ppm
...
Z_{ij12}	Month 12	Latitude (91 × 1)	CO ₂ Concentration (91 × 144)	372.3 ppm
N_{ij1}	Month 1	Latitude (91 × 1)	Count (91 × 144)	259
N_{ij2}	Month 2	Latitude (91 × 1)	Count (91 × 144)	264
...
N_{ij12}	Month 12	Latitude (91 × 1)	Count (91 × 144)	290
σ_{zij1}	Month 1	Latitude (91 × 1)	Standard Deviation (91 × 144)	4.09 ppm
σ_{zij2}	Month 2	Latitude (91 × 1)	Standard Deviation (91 × 144)	4.06 ppm
...
σ_{zij12}	Month 12	Latitude (91 × 1)	Standard Deviation (91 × 144)	3.84 ppm
μ_{ij}	0	0	Trend (91 × 144)	2.174 ppm/year
A_{ij}	0	0	Intercept (91 × 144)	373.5 ppm
$\sigma_{\mu ij}$	0	0	Trend Uncertainty (91 × 144)	0.26 ppm/year
M_{ij}	0	0	Number in Trend (91 × 144)	96

7. SUMMARY AND CONCLUSIONS

A set of monthly representations of mid-tropospheric carbon dioxide from the AIRS instrument were produced that include the monthly CO₂ concentration averaged over all years for each 2.0° × 2.5° bin for all latitudes above -60°. The distribution and time dependence in the representations clearly show a seasonal dependence of amplitude and phase indicative of inter-hemispherical transport. Also included in the file are the standard deviation and number of individual retrievals that fell in the bin. A trend matrix is provided that allows for reconstruction of the original AIRS L3 CO₂ monthly data series. Reconstruction error over all points in the data set is 1.48 ppm one-sigma with less than 2% outliers. The statistical significance of the representations are very high with critical values, α , lower than 0.2 for most months and regions on the globe. The trends in a given bin, while suggestive of regional sources and sinks, are marginally significant. When averaged to a zonal scale, we improve the confidence in the mean trend and see trends lowest in the tropics and highest in the northern hemisphere and the arctic region. While we expect this dependency based on the global distribution of surface vegetation and industrialization, further characterization of the latitudinal covariance and validation is required to confirm these findings.

ACKNOWLEDGMENTS

The research described in this paper was carried out at the Jet Propulsion Laboratory, California Institute of Technology, under a contract with the National Aeronautics and Space Administration.

REFERENCES

- [1] Aumann, H. H., Chahine, M. T., Gautier, C., Goldberg, M. D., Kalnay, E., McMillin, L. M., Revercomb, H., Rosenkranz, P. W., Smith, W. L., Staelin, D. H., Strow, L. L., Susskind, J., "AIRS/AMSU/HSB on the Aqua mission: design, science objectives, data products, and processing systems," *Geoscience and Remote Sensing, IEEE Transactions on*, 41(2), 253–264 (2003).
- [2] Chahine, M., Barnet, C., Olsen, E. T., Chen, L. and Maddy, E., "On the determination of atmospheric minor gases by the method of vanishing partial derivatives with application to CO₂," *Geophys. Res. Lett.* 32, L22803, doi:10.1029/2005GL024165, (2005).
- [3] Chahine, M. T., Chen, L., Dimotakis, P., Jiang, X., Li, Q., Olsen, E. T., Pagano, T., Randerson, J. and Yung, Y. L., "Satellite remote sounding of mid-tropospheric CO₂," *Geophys. Res. Lett.* 35, L17807, doi:10.1029/2008GL035022, (2008).
- [4] Jiang, K., Chahine, M. T., Olsen, E. T., Chen, L. L. and Yung, Y. L., "Interannual variability of mid-tropospheric CO₂ from Atmospheric Infrared Sounder," *Geophys. Res. Lett.* 37, L13801, doi:10.1029/2010GL042823, (2010).
- [5] Li, K. F., Tian, B., Waliser, D. E., Yung, Y. L., "Tropical mid-tropospheric CO₂ variability driven by the Madden-Julian oscillation," *PNAS* 107(45), 19171–19175, doi:10.1073/pnas.1008222107, (2010).
- [6] Tiwari, Y. K., Gloor, M., Engelen, R. J., Chevallier, F., Rodenbeck, C., Korner, S., Peylin, P., Braswell, B. H. and Heimann, M., "Comparing CO₂ retrieved from Atmospheric Infrared Sounder with model predictions: Implications for constraining surface fluxes, and lower-to-upper troposphere transport," *J. Geophys. Res.* 111, D17106, doi:10.1029/2005JD006681, (2006).
- [7] Feng, L., Palmer, P. I., Yang, Y., Yantosca, R. M., Kawa, S. R., Paris, J.-D., Matsueda, H., Machida, T., "Evaluating a 3-D transport model of atmospheric CO₂ using ground-based, aircraft, and space-borne data," *Atmos. Chem. Phys.* 11, 2789–2803, 2011, doi:10.5194/acp-11-2789-2011, (2011).
- [8] Pagano, T. S., et al., "Seven years of observations of mid-tropospheric CO₂ from the Atmospheric Infrared Sounder," *Acta Astronautica*, doi:10.1016/j.actaastro.2011.05.016, (2011).
- [9] Bai, W. G., Zhang, X. Y., Zhang, P., "Temporal and spatial distribution of tropospheric CO₂ over China based on satellite observations," *Chinese Science Bulletin* 55(31), 3612–3618, doi: 10.1007/s11434-010-4182-4, (2010).
- [10] Weatherhead, E., et al., "Factors affecting the detection of trends: Statistical considerations and applications to environmental data," *J. Geophys. Res.* 103, D14, 17149–17161, (1998).